Buckling of Carbon Honeycombs – A New Mechanism for Molecular Mass Transportation

Jin Zhang[1*], Chengyuan Wang[2*]

[1] Shenzhen Graduate School, Harbin Institute of Technology, Shenzhen 518055, China

[2] Zienkiewicz Centre for Computational Engineering, College of Engineering, Swansea University, Bay Campus, Fabian Way, Swansea, Wales SA2 8EN, UK

Abstract: Buckling of carbon honeycombs (CHCs) under uniaxial compression is studied based on molecular dynamics simulations. The uniaxial load applied to CHCs finally induces the local buckling associated with the biaxial compression state. This phenomenon originates from the residual stress in the CHCs due to the edge effect of component graphene nanoribbons. Under such a biaxial stress state, CHCs are found to exhibit two topographically different buckling modes when subjected to the uniaxial compression in the armchair and zigzag directions, respectively. In particular, the nonlocal effect originating from van der Waals interactions greatly reduces the ability of CHCs to resist structural instability and leads to early onset of CHC buckling. The buckling of CHCs is expected to be instrumental in the future applications of CHC structures. As an example, we show that an effective transportation of molecular mass enabled by the local buckling of CHCs is promising for the future CHC-based gas storage. In particular, the key issue to implement the transportation of the adsorbed gas molecules inside CHCs is to optimise the geometric size of CHCs in favour of the local buckling rather than the global buckling.

[*]Corresponding authors.

E-mail address: jinzhang@hit.edu.cn (J. Zhang); chengyuan.wang@swansea.ac.uk. (C. Wang).

1. Introduction

The discovery of novel carbon allotropes such as zero-dimensional fullerene, one-dimensional carbon nanotube (CNT) and two-dimensional graphene has triggered intense research on various carbon-based nanomaterials (CBNs). In the past decades, the studies were mainly focused on revealing the physical and chemical properties of these CBNs.[1-4] Recently, efforts have been shifted to the design of carbon-based super-architectures constructed by the units of fullerene, CNT and graphene.[5-15] A typical example is the most recently synthesised three-dimensional carbon honeycomb (CHC) structure comprising of the element of graphene.[10] It was assumed in the experiment[10] that a CHC structure consists of zigzag-edged graphene nanoribbons and the three adjacent nanoribbons are linked together by a line of sp^2-bonded carbon atoms. However, recent theoretical studies indicated that a CHC structure is stable only when the junctions are formed by sp^3 rather than sp^2 bonding.[16, 17] Actually, the first theoretical report of these CHC structures by Karfunkel and Dressler[11] can be dated back to 1992 and then followed by a series of investigations on their structural stability.[12-15]

Nevertheless, the computational simulations on the material properties of CHCs were not available in the literature until very recently. For example, *ab initio* simulations, first-principles calculations and molecular dynamics (MD) simulations have been employed to characterize the formation energies, electronic properties, thermal properties, magnetic properties and mechanical properties of CHCs.[12-20] The results show that CHCs possess high structural stability comparable to the most stable phases of carbon materials (graphite and diamond).[15] Recent MD simulations reveal that CHCs have a very high thermal conductivity.[17-19] In addition, the electronic band structure and electronic density of states of CHCs are found to be size-dependent, similar to their nanotube counterparts.[15] Moreover, the elastic properties of CHCs calculated in the density-functional-based tight-binding method[15] and MD simulations[16] are found to be in the range

between the values of graphite and diamond. The mass densities of the CHC are smaller than those of the graphite.[13] These unique properties make CHCs promising for a broad range of applications in next-generation nanodevices and nanocomposites. In particular, CHCs are proven to have great potential for the gas storage due to their low density and large surface area per unit mass.[10, 15, 18, 21, 22]

On the one hand, the potential gas storage application requires CHCs to resist the buckling due to mechanical loads. This becomes a major issue as the component graphene element in CHCs is the thinnest film in the world associated with a very small bending modulus. Thus CHCs are prone to buckle due to the compression which unfortunately happens to be the loading sustained by CHCs in the gas storage. Actually, the buckling instability is a common failure mechanism of CBNs, which was also observed in other CBNs, including CNTs,[23-30] carbon nanoscrolls,[31, 32] graphene sheets,[33, 34] and CNT networks.[35] The buckling behaviours of these CBNs have been well investigated to date. Nevertheless, little is known about the buckling behaviours of the newly fabricated CHCs. On the other hand, although many studies have revealed that CHCs possess high storage capacity for gas molecules,[10, 18, 21, 22] how to shuttle the gas molecules adsorbed inside CHCs is another crucial but largely unexplored issue for the success of CHC-based gas storage. This has been unclear until recent studies on CNTs and carbon nanoscrolls showing that the buckling of CBNs provided an effective atomic transportation mechanism.[31, 36, 37] Inspired by these research progresses we are interested in studying the gas molecules transportation via CHC buckling. The above discussions show that an in-depth understanding of the buckling behaviour is essential for the successful application of CHCs.

In this paper, the buckling instability of CHCs under uniaxial compression has been studied by MD simulations. Two topographically different buckling modes have been detected when the

external compression on CHCs is applied along different directions. Then, effort was invested to reveal the physical mechanisms behind the unique behaviours via a theoretical analysis. In addition, a case study was conducted showing that the local buckling of CHCs can be employed as an efficient means to transport the gas molecules adsorbed inside the CHCs. This may provide a new avenue to the development of CHC-based nanotechnology for molecular transportation.

2. MD simulations on CHCs

As a sophisticated modelling technique for nanomechanics, MD simulations have been widely accepted in studying the structural instability of various CBNs including CNTs, carbon nanoscrolls and graphene sheets.[23-25, 27-29, 31-33] In present study, classical MD simulations will be adopted to study the buckling behaviours of CHCs. Here, we considered a CHC structure consisting of zigzag-edged graphene nanoribbons (see Figure 1a). In the CHCs studied here all three adjacent nanoribbons were linked by a line of sp^3-bonded carbon atoms. The structure of such a triple junction is shown in the Supporting Information (Figure S1) and proven to be stable in pervious theoretical studies.[16, 17] In the present simulations, the interactions between two carbon atoms were described by the adaptive intermolecular reactive empirical bond order (AIREBO) potential,[38] which is able to well represent the thermal and elastic properties of CHC structures.[16, 18] During the simulations, CHCs were firstly relaxed to a minimum energy state using the conjugate gradient algorithm. Then MD simulations were performed with the following procedure. First, CHCs were completely relaxed for a certain period (20 ps was used in this step) to minimize the internal energy and reach an equilibrium state. In doing this, the NVT ensemble (constant number of particles, volume and temperature) with the aid of the Nosé-Hoover thermostat algorithm[39] was employed to maintain a constant temperature. In the present study, the system

temperature was set at 1 K to reduce the random thermal fluctuation effect. Moreover, the velocity Verlet integration algorithm with the time step of 0.5 fs was utilized to integrate Hamiltonian equations of motion determined by Newton's second law. After the full relaxation, the CHCs were quasi-statically loaded under uniaxial compression. To reach this goal, one end of the CHCs was fixed and the opposite end was pushed along the *x* or *y* direction (see Figure 1). This created a ramp velocity profile where the velocity rises from zero at the fixed end to its maximum value at the free end. To avoid the crystalline defects normally produced due to a high rate of loading we chose a relatively low strain rate of 0.001 ps^{-1} in the present simulations. Finally, the system was relaxed for 1 ps to allow the CHC to reach a new equilibrium state. In this step the axial stress σ taken as the arithmetic mean of the local stresses on all atoms was recorded. Here σ is defined as follows:[40]

$$\sigma = \frac{1}{N}\sum_{i=1}^{N}\frac{1}{V_i}\left(m_i v_a^i v_a^i + \frac{1}{2}\sum_{j\neq i}^{N} F_a^{ij} r_a^{ij} \right), \tag{1}$$

where m_i is the mass of atom *i*, v_a^i is the axial velocity of atom *i*, F_a^{ij} refers to the axial interatomic force between atoms *i* and *j*, r_a^{ij} is the interatomic distance in the axial direction between atoms *i* and *j*, V_i refers to the volume of atom *i*, which was assumed as a hard sphere in a closely packed undeformed crystal structure, and N is the number of atoms.

By repeating the above process, a CHC is compressed continuously until the required strain or stress has been obtained. In the present study, all MD simulations were conducted using a large-scale atomic/molecular massively parallel simulator (LAMMPS)[41] with non-periodic boundary conditions in all directions.

3. Results and discussion

In this section we will study the buckling behaviour of CHCs based on the MD technique detailed above. Unless otherwise specified, in this study we will consider a CHC whose length in the *x* direction, i.e., L_x in Figure 1b, is 30 Å, length in the *y* direction, i.e., L_y in Figure 1b, is 37 Å and thickness *t* is 7.5 Å. The cell length *l* (or the length of the component graphene element) of the CHC is 3.55 Å. We can see from Figure 1b that a CHC shows a "zigzag" configuration along the *x* direction and an "armchair" configuration along the *y* direction. The distinct configurations of CHCs along the *x* and *y* directions suggest that CHCs could be an anisotropic structure with different mechanical properties in the *x* and *y* directions. Motivated by this idea, in this section we will study the influence of the configuration on the mechanical responses of CHCs subjected to compression in the *x* and *y* directions, respectively.

3.1 Buckling modes in CHCs

In Figure 2a we show the stress-strain relation for the CHC when it is compressed along the *y* direction. Here, the circle-marked line and square-marked line represent the results obtained in the presence and absence of the van der Waals (vdW) interaction, respectively. The snapshots of the tested CHC at different compression stages are shown in Figure 2b-2e. Each of them represents a critical point marked on the stress-strain curves in Figure 2a. Initially, the stress monotonically increases with growing strain, showing the pre-buckling deformation of the compressed CHC. At this stage, no significant change is observed for the configuration of the compressed CHC (Figure 2b) and the stress-strain curves represented by the circle-marked and square-marked lines coincide with each other (Figure 2a), giving negligible influence of the vdW interaction.

Further raising the strain up to a certain critical value results in a sudden jump of the stress, signifying the onset of the initial local buckling in the CHC. The buckling mode is shown in Figure 2c, which is similar to the buckling deformation reported by Zhang et al.[16] in their very recent studies of CHC mechanics and the one achieved for the macroscopic honeycomb structures under a uniaxial compression.[42] Here, the strain at the onset of CHC buckling is defined as the critical buckling strain ε_{cr} and the associated stress is referred to as the critical buckling stress σ_{cr}. From Figure 2a we can see that σ_{cr} obtained by considering the vdW interaction is 13.8 GPa which is 10% smaller than σ_{cr} calculated without the vdW interaction. The lower σ_{cr} obtained for the CHC is possibly due to the so-called nonlocal effect originating from the long range vdW interaction considered.[43] In fact, Figure 2c shows that the local buckling of the CHC is triggered by the Euler buckling of its component graphene elements. As shown in Figure 1 and pointed in ref 10 the characteristic length of the component graphene elements in CHCs (i.e., l in Figure 1b) is usually very small. Thus the corresponding nonlocal effect is higher leading to lower Euler buckling load of the component graphene elements[43-45] and accordingly, the smaller σ_{cr} of the CHC structure. Specifically, as explained in ref 45, the nonlocal constant (e_0a) reflects the pre-stress in the component graphene due to the long range vdW interaction.[43]

After the initial CHC buckling, we see a strain hardening effect where further enhancing the compressive stress yields a greater strain. In particular, the same increment of the strain requires a higher stress in the presence of the vdW force. Thus the slope of the circle-marked line (with the vdW interaction) is greater than the slope of the square-marked line (without the vdW interaction). When the strain further increases to a critical value (0.26), another sudden drop of stress, i.e., the second buckling, is observed for the CHC when the vdW interaction is considered. This leads to a topographically change shown in Figure 2d where the global buckling mode is

achieved, which is characterised by the sideways deformation of the whole CHC structure. On the other hand, the (second) global buckling does not occur for the CHC when the vdW interaction is not taken into considered (see Figure 2e). Form these results it follows that the vdW interaction or the nonlocal effect has no influence the pre-buckling properties of CHCs when there is the uniform deformation without any strain gradient. It however significantly affects the buckling and post-buckling behaviours of CHCs when the non-uniform deformation appears with large strain gradients. This phenomenon can be well understood by the Eringen's nonlocal elastic theory,[43] where the gradient-dependent constitutive equations are introduced to represent the nonlocal effect at the nanoscale.[43] Our results to some extent confirm that the vdW interaction exerts the influence on the mechanics of CHCs via the nonlocal effect or the physical origin of the nonlocal effect on CHCs is the vdW interaction between carbon atoms.

Next, we will study the mechanical response of CHCs when they are compressed along the *x* direction. Similar to Figure 2a, we see from Figure 3a that when the CHC is compressed along the *x* direction the monotonic increase with rising strain is observed for the stress with no significant change in the configuration of the CHC (see Figure 3b). When the strain rises to a critical value the stress is found to suddenly drop, showing the occurrence of the initial local buckling. The local buckling mode of the CHCs is shown in Figure 3c, which is found to be topographically different from the buckling mode of CHCs compressed in the *y* direction (see Figure 2c). In the post-buckling process the second abrupt drop in stress is also observed, corresponding to the global buckling of the entire CHC structures (see Figure 3d).

In the present study, attention is mainly focused on the buckling modes of pristine CHCs. However, defects such as vacancy and Stone-Wales (SW) defects may appear during the fabrication of CBNs.[46] In a very recent MD simulation on CHCs, the SW defect is found to

decrease the critical buckling load but its influence on the buckling mode is trivial.[16] To further study the effect of the vacancy, another common defect observed in CBNs, we have performed MD simulations on the buckling of CHCs in the presence of vacancies (see Figure S2 in the Supporting Information). The simulations show that, the critical buckling stress of the defective CHCs is reduced by 8.5% and 10.3%, respectively, relative to that of pristine CHCs when they are compressed along the *x* and *y* directions. The buckling mode however is topographically similar to that of pristine CHCs. These behaviours are detected in most cells of the defective CHCs except for a few nearby the defect (see Figure S2 in the Supporting Information) and consistent with the observations in ref 16 for the SW defects.

According to the previous theoretical and experimental studies on the macroscopic honeycomb structures,[42, 47] no local buckling occurs for the honeycomb compressed uniaxially along the *x* (zigzag) direction. This is confirmed in our finite element (FE) simulations on macroscopic honeycombs but contrasts the present MD simulations on the nanoscale CHC, where the local buckling is achieved. In the present study, the FE calculations were carried out using the commercial code ANSYS. In this process, BEAM3 element was selected to describe the elastic wall of the honeycomb structure. The FE model and the buckling analysis method are detailed in the Supporting Information. To explain the discrepancy due to the length scale change, we showed in Figure 4a the stress distribution of a CHC after the initial structural relaxation. The residual compression is detected for the CHC, which is thought of being a result of the edge effect in the component graphene element.[48, 49] In the present study the residual compressive stress is detected to be around -0.93 GPa. This residual compressive stress is smaller than the critical buckling stress σ_{cr}, but may significantly affect the buckling behaviours, since it is of the same order of magnitude of σ_{cr}. In the presence of the residual compressive stress, the CHC is actually subjected to an

equivalent biaxial compression when the uniaxial external compression is applied. Specifically, when the external load is applied in the *y* direction, the resultant stress in the *y* direction (σ_{yy}) should be larger than the one in the *x* direction (σ_{xx}), i.e., $\sigma_{yy} > \sigma_{xx}$ or vice versa, i.e., $\sigma_{xx} > \sigma_{yy}$.

Based on FE simulations, in Figure 4b and 4c we showed the buckling modes of the honeycomb structures under the two biaxial compression states, i.e., $\sigma_{yy} > \sigma_{xx}$ and $\sigma_{xx} > \sigma_{yy}$. It is noted that when $\sigma_{yy} > \sigma_{xx}$, the buckling mode obtained in FE simulations is similar to the one of the CHC compressed in the *y* direction only (see Figure 2c). The good agreement is also achieved between the two cases for $\sigma_{xx} > \sigma_{yy}$ (see Figures 3c and 4c). These comparison results indicated that the residual stress in CHCs should be taken into consideration in the buckling analysis of the CHCs. In other words, an equivalent biaxial compression state should be considered even if an external load is applied in only one direction. The biaxial compression the CHCs leads to different buckling modes, depending on the direction of the applied compression.

3.2 Molecular transportation via CHC local buckling

As reviewed in the introduction, CHCs have great potential for gas storage due to their high porosity and accessibility.[10, 15, 18, 21, 22] For example, it is shown that CHCs possess high storage capacity for hydrogen (H_2) molecules[21] and carbon dioxide (CO_2) molecules.[18] Such a gas storage application of CHCs requires them to sustain the mechanical load without buckling. Another crucial but largely unexplored issue for this application is how to shuttle the gas molecules adsorbed inside CHCs. In what follows, taking the hydrogen gas molecules as an example we will demonstrate an effective mechanism of molecular mass transportation enabled by the local buckling of CHCs. In this simulation, a CHC was initially immersed in a hydrogen reservoir whose pressure was kept at 1 MPa. After that, two hydrogen molecules were found to adsorb in each cell

of CHCs (see Figure 5), which corresponds to a gravimetric hydrogen uptake of 1.04 wt. %. It is noted that the gas storage capacity of CHCs strongly depends on the cell size of CHCs: CHCs with larger cell possess larger storage capacity.[18, 21] Thus, the hydrogen storage capacity of CHCs can be raised by increasing the cell size of CHCs. In this study, the non-bonded vdW interactions of carbon-hydrogen were simulated by the Lennard-Jones atomic pair potential: $V = 4\delta[(\sigma / r)^{12} - (\sigma / r)^{6}]$. Here, r is the hydrogen-carbon atomic pair distance, δ = 0.003 eV and σ = 3.18 Å.[50]

Firstly we will compress the CHCs adsorbed with hydrogen along the *y* direction. The stress-strain relation during the compression process is plotted in Figure 6a. Similar to the CHCs without hydrogen (Figure 2a), we can see from Figure 6a that the stress initially increases with increasing strain linearly and then suddenly falls down when the stress (or strain) reaches a critical value σ_{cr} (or ε_{cr}), corresponding to the local buckling of CHCs. Compared with the CHCs without hydrogen, the present CHCs adsorbed with hydrogen is found to be more stable, since σ_{cr} = 20 GPa in Figure 6a is much larger than 13.8 GPa obtained in Figure 2a. The enhanced σ_{cr} is attributed to the repulsive interaction between the central hydrogen molecule and its surrounding carbon atoms in the cell wall (graphene element) of the CHCs. In Figure 6b we present the residual stress in the CHCs adsorbed with hydrogen before the external compressive stress is applied. Comparing this figure with Figure 4a we can see that due to the effect of the repulsive interaction the residual stress in the CHCs adsorbed with hydrogen is much smaller than that in the CHCs without hydrogen. The smaller residual compressive stress in CHCs will thus raise the critical buckling stress of CHCs.

In Figure 6c and 6d we show the configuration of the CHCs adsorbed with hydrogen just before and after the buckling. We can see from Figure 6c that before the CHC buckles all hydrogen

molecules can adsorb inside the CHC just like the case without external compression (see Figure 5). However, after the CHC buckles, the shape of the cell in the CHC will topographically change, resulting in the decrease of the size of the cell. Decreasing size of the cell of the CHC imposes increasing repulsive net forces on the adsorbed hydrogen molecules due to the nature of hydrogen-carbon vdW interaction. As a result, it is observed in Figure 6d that up to 91% of the hydrogen molecules were pushed outside the CHC after the CHC buckles. After releasing the external compression and relaxing the CHC again, the CHC can recover to its initial configurations. In other words, such a CHC-based gas storage can be used repetitively without causing any damages. From above analysis, we see that the local buckling of CHCs offers an efficient technique to transport the gas molecules adsorbed inside the CHCs.

Next, we will compress the CHCs adsorbed with hydrogen along the *x* direction. An abrupt drop of the stress is also detected in the stress-strain curve shown in Figure 7a. However, in Figure 7c this stress drop corresponds to a global buckling rather than a local buckling. In other words, the local buckling instability will not occur for the CHC (filled with hydrogen) subject to a uniaxial compression in the *x* direction. As we illustrated in Section 3.1 a compression along the *x* direction leads to the local buckling only when CHCs are under a biaxial compression state. As for the CHCs without hydrogen, they are under the biaxial compression state even an external compression is imposed in one direction. On the other hand, when the hydrogen molecules are inserted into the cell of the CHCs, the hydrogen-carbon vdW interaction will induce the repulsive net forces on the cell wall (component graphene element), which will greatly decrease the residual compressive stress in the CHCs (see Figure 6b) and can even turn the residual compressive stress into a tensile stress. Under this circumstance, the CHC is subjected to a compression only along the *x* direction where the load is applied. The local buckling instability thus will not occur for the hydrogen filled

CHCs compressed in the *x* direction only. Thus, in Figure 7c the hydrogen molecules still stay inside the CHCs even after the global buckling of CHCs. This is because that the global buckling of the CHCs occurs without local distortion of the CHCs and thus cannot reduce the cell size significantly to squeeze the hydrogen out. Comparing Figure 7c with Figure 6d we can come to the conclusion that only the local buckling rather than the global buckling of the CHCs can be employed to transport the gas molecules adsorbed inside the CHCs. Moreover, it is also found that compression in the *y* direction is more efficient than the one along the *x* direction in generating the local buckling. The *x* direction compression may not lead to the local buckling due to the repulsive interaction between the adsorbed molecules and the surrounding carbon atoms on the cell wall. It is worth pointing out that the mechanism demonstrated in this paper may also have impacts on the transportation of other molecules, such as water molecules, fullerenes, nanoparticles, and deoxyribonucleic acids, as the transportation mechanism proposed here is essentially driven by the nonbonded vdW interaction of the molecules and the cell wall of CHCs.

To utilize the local buckling for transporting the gas molecules, we may optimize the geometry of the CHCs firstly to induce the local buckling rather than the global buckling. Previous studies on CNT buckling show that the local-to-global buckling mode transition of nanostructures is largely determined by their aspect (length-to-thickness) ratio.[25, 27-29] Therefore, considering a uniaxial compression along the *y* direction we have investigated the influence of the geometric size on the buckling behaviours of CHCs by changing their length L_y or thickness *t*. In Figure 8 we plotted the critical buckling stress σ_{cr} with respect to the length-to-thickness ratio (L_y / t). We can see from this figure that there exists a critical value 10.5 for L_y / t, determining whether the buckling of the CHCs is local buckling or global buckling. When $L_y / t < 10.5$, the local buckling instability occurs in CHCs. In this case σ_{cr} is found to be almost independent with L_y / t and

remains a constant around a mean value 14 GPa when L_y / t increases from 3.42 to 10.21, since in this process the deviation of σ_{cr} from this average value is less than 3%. The L_y / t-independent σ_{cr} achieved here is due to the fact that σ_{cr} in this case is a parameter corresponding to the local buckling behaviour of the CHCs and thus is almost independent of the global parameters of CHCs, e.g., the length-to-thickness ratio L_y / t considered here. When $L_y / t > 10.5$, we can see from Figure 8 that CHCs hold a global column-like buckling. In this case, σ_{cr} is found to decrease with increasing L_y / t. For example, σ_{cr} decreases from 12.05 GPa to 5.94 GPa when L_y / t increases from 11.25 to 15.8. As for the global column-like buckling of the CHC, its critical buckling stress can be theoretically predicted based on the well-known Euler buckling theory,[51] i.e., $\sigma_{cr} = (\pi^2 E / 3) \cdot (L_y / t)^{-2}$, where E is the effective Young's modulus of the CHC. The Euler buckling theory shows that $\sigma_{cr} \propto (L_y / t)^{-2}$, which matches the MD simulation results very well (see the solid line in Figure 8).

4. Conclusions

Based on MD simulations we have studied the buckling behaviours of CHCs subjected to uniaxial compression. The residual compressive stress is found in CHCs due to the edge effect of the component graphene element. It results in a biaxial compression on the CHCs when compression is applied in armchair or zigzag direction. When the applied uniaxial compression exceeds a critical value, CHCs will exhibit two topographically different local buckling modes associated with the equivalent biaxial compression. It is found that the critical buckling stress (strain) is greatly reduced due to the nonlocal effect originating from the vdW interaction in CHCs.

The local buckling of CHCs is shown to be an efficient means to transport the gas molecules adsorbed inside the CHCs, which is promising for the future gas storage application based on CHCs. To implement this technique, the length-to-thickness ratio of the CHCs should be kept smaller than a critical value to induce the local buckling that is necessary for the transportation of gas molecules inside the CHCs.

Acknowledgements

This work was supported by the National Natural Science Foundation of China (No. 11602074). J.Z. also wishes to acknowledge the financial support from Harbin Institute of Technology (Shenzhen Graduate School) through the Scientific Research Starting Project for New Faculty.

Supporting Information

Details of FE simulations for the buckling analysis of honeycomb structures and some supporting figures.

References

(1) Castro Neto, A. H.; Guinea, F.; Peres, N. M. R.; Novoselov, K. S.; Geim, A. K. The Electronic Properties of Graphene. *Rev. Mod. Phys.* **2009**, 81, 109-162.

(2) Lee, C. G.; Wei, X. D.; Kysar, J. W.; Hone, J. Measurement of the Elastic Properties and Intrinsic Strength of Monolayer Graphene. *Science* **2008**, 321, 385-388.

(3) Robertson, J. Realistic Applications of CNTs. *Mater. Today* **2004**, 7, 46-52.

(4) Kis, A.; Zettl, A. Nanomechanics of Carbon Nanotubes. *Phil. Trans. R Soc. A* **2008**, 366, 1592-1611.

(5) Chernozatonskii, L.; Richter, E.; Menon, M. Crystals of Covalently Bonded Carbon Nanotubes: Energetics and Electronic Structures. *Phys. Rev. B* **2002**, 65, 241404(R).

(6) Zhou, R. L.; Liu, R.; Li, L.; Wu, X. J.; Zeng, X. C. Carbon Nanotube Superarchitectures: An Ab Initio Study. *J. Phys. Chem. C* **2011**, 115, 18174-18185.

(7) Ueda, S.; Ohno, K.; Noguchi, Y.; Ishii, S.; Onoe, J. Dimensional Dependence of Electronic Structure of Fullerene Polymers. *J. Phys. Chem. B* **2006**, 110, 22374-22381.

(8) Yamanaka, S.; Kubo, A.; Inumaru, K.; Komaguchi, K.; Kini, N. S.; Inoue, T.; Irifune, T. Electron Conductive Three-Dimensional Polymer of Cuboidal C_{60}. *Phys. Rev. Lett.* **2006**, 96, 076602.

(9) Romo-Herrera, J. M.; Terrones, M.; Terrones, H.; Dag, S.; Meunier, V. Covalent 2D and 3D Networks from 1D Nanostructures: Designing New Materials. *Nano Lett.* **2007**, 7, 570-576.

(10) Krainyukova, N. V.; Zubarev, E. N. Carbon Honeycomb High Capacity Storage for Gaseous and Liquid Species. *Phys. Rev. Lett.* **2016**, 116, 055501.

(11) Karfunkel, H. R.; Dressler, T. New Hypothetical Carbon Allotropes of Remarkable Stability Estimated by MNDO Solid-State SCF Computations. *J. Am. Chem. Soc.* **1992**, 114, 2285-2288.

(12) Park, N.; Ihm, J. Electronic Structure and Mechanical Stability of the Graphitic Honeycomb Lattice. *Phys. Rev. B* **2000**, 62, 7614-7618.

(13) Umemoto, K.; Saito, S.; Berber, S.; Tománek, D. Carbon Foam: Spanning the Phase Apace between Graphite and Diamond. *Phys. Rev. B* **2001**, 64, 193409.

(14) Ribeiro, F. J.; Tangney, P.; Louie, S. G.; Cohen, M. L. Structural and Electronic Properties of Carbon in Hybrid Diamond-Graphite Structures. *Phys. Rev. B* **2005**, 72, 214109.

(15) Kuc, A.; Seifert, G. Hexagon-Preserving Carbon Foams: Properties of Hypothetical Carbon Allotropes. *Phys. Rev. B* **2006**, 74, 214104.

(16) Zhang, Z.; Kutana, A.; Yang, Y.; Krainyukova, N. V.; Penev, E. S.; Yakobson, B. I. Nanomechanics of Carbon Honeycomb Cellular Structures. *Carbon* **2017**, 113, 26-32.

(17) Pang, Z. Q.; Gu, X. K.; Wei, Y. J.; Yang, R. G.; Dresselhaus, M. S. Bottom-up Design of Three-Dimensional Carbon-Honeycomb with Superb Specific Strength and High Thermal Conductivity. *Nano Lett.* **2017**, 17, 179-185.

(18) Gao, Y.; Chen, Y.; Zhong, C.; Zhang, Z.; Xie, Y.; Zhang, S. Electron and Phonon Properties and Gas Storage in Carbon Honeycombs. *Nanoscale* **2016**, 8, 12863-12868.

(19) Wei, Z. Y.; Yang, F.; Bi, K. D.; Yang, J. K.; Chen, Y. F. Thermal Transport Properties of All-sp^2 Three-Gimensional Graphene: Anisotropy, Size and Pressure Effects. *Carbon* **2017**, 113, 212-218.

(20) Yu, G. D.; Jiang, L. W.; Zheng, Y. S. Surface Magnetism of the Carbon Foam: An Ab-Initio Theoretical Study. *Appl. Phys. Lett.* **2014**, 105, 061601.

(21) Park, N.; Hong, S.; Kim, G.; Jhi, S. H. Computational Study of Hydrogen Storage Characteristics of Covalent-Bonded Graphenes. *J. Am. Chem. Soc.* **2007**, 129, 8999-9003.

(22) Krainyukova, N. V. Capturing Gases in Carbon Honeycomb. *J. Low Temp. Phys.* **2017**, 187, 90-104.

(23) Yakobson, B. I.; Brabec, C. J.; Bernholc, J. Nanomechanics of Carbon Tubes: Instabilities beyond Linear Response. *Phys. Rev. Lett.* **1996**, 76, 2511-2514.

(24) Liew, K. M.; Wong, C. H.; He, X. Q.; Tan, M. J.; Meguid, S. A. Nanomechanics of Single and Multiwalled Carbon Nanotubes. *Phys. Rev. B* **2004**, 69, 115429.

(25) Wang, Y.; Wang, X. X.; Ni, X. G.; Wu, H. A. Simulation of the Elastic Response and the Buckling Modes of Single-Walled Carbon Nanotubes. *Comput. Mater. Sci.* **2005**, 32, 141-146.

(26) Yap, H. W.; Lakes, R. S.; Carpick, R. W. Mechanical Instabilities of Individual Multiwalled Carbon Nanotubes under Cyclic Axial Compression. *Nano Lett.* **2007**, 7, 1149-1154.

(27) Feliciano, J.; Tang, C.; Zhang, Y. Y.; Chen, C. F. Aspect Ratio Dependent Buckling Mode Transition in Single-Walled Carbon Nanotubes under Compression. *J. Appl. Phys.* **2011**, 109, 084323.

(28) Zhang, Y. Y.; Wang, C. M.; Duan, W. H.; Xiang, Y.; Zong, Z. Assessment of Continuum Mechanics Models in Predicting Buckling Strains of Single-Walled Carbon Nanotubes. *Nanotechnology* **2009**, 20, 395707.

(29) Wang, C. M.; Zhang, Y. Y.; Xiang, Y.; Reddy, J. N. Recent Studies on Buckling of Carbon Nanotubes. *Appl. Mech. Rev.* **2010**, 63, 030804.

(30) Shima, H. Buckling of Carbon Nanotubes: A State of the Art Review. *Materials* **2012**, 5, 47-84.

(31) Zhang, Z.; Huang, Y. J.; Li, T. Buckling Instability of Carbon Nanoscrolls. *J. Appl. Phys.* **2012**, 112, 063515.

(32) Song, H. Y.; Geng, S. F.; An, M. R.; Zha, X. W. Atomic Simulation of the Formation and Mechanical Behavior of Carbon Nanoscrolls. *J. Appl. Phys.* **2013**, 113, 164305.

(33) Duan, W. H.; Gong, K.; Wang, Q. Controlling the Formation of Wrinkles in a Single Layer Graphene Sheet Subjected to In-Plane Shear. *Carbon* **2011**, 49, 3107-3112.

(34) Deng, S. K.; Berry, V. Wrinkled, Rippled and Crumpled Graphene: An Overview of Formation Mechanism, Electronic Properties, and Applications. *Mater. Today* **2016**, 19, 197-212.

(35) Li, Y.; Qiu, X. M.; Yin, Y. J.; Yang, F.; Fan, Q. S. The Elastic Buckling of Super-Graphene and Super-Square Carbon Nanotube Networks. *Phys. Lett. A* **2010**, 374, 1773-1778.

(36) Insepov, Z.; Wolf, D.; Hassanein, A. Nanopumping Using Carbon Nanotubes. *Nano Lett.* **2006**, 6, 1893-1895.

(37) Wang, Q. Atomic Transportation via Carbon Nanotubes. *Nano Lett.* **2009**, 9, 245-249.

(38) Stuart, S. J.; Tutein, A. B.; Harrison, J. A. A Reactive Potential for Hydrocarbons with Intermolecular Interactions. *J. Chem. Phys.* **2000**, 112, 6472-6486.

(39) Nosé, S. A Unified Formulation of the Constant Temperature Molecular Dynamics Methods. *Chem. Phys.* **1984**, 81, 511-519.

(40) Zimmerman, J. A.; Webb III, E. B.; Hoyt, J. J.; Jones, R. E.; Klein, P. A.; Bammann, D. J. Calculation of Stress in Atomistic Simulation. *Modell. Simul. Mater. Sci. Eng.* **2004**, 12, S319-S332.

(41) Plimpton, S. J. Fast Parallel Algorithms for Short-Range Molecular Dynamics. *J. Comput. Phys.* **1995**, 117, 1-19.

(42) Gibson, L. J.; Ashby, M. F.; Zhang, J.; Triantafillou, T. C. Failure Surfaces for Cellular Materials under Multiaxial Loads—I. Modelling. *Int. J. Mech. Sci.* **1989**, 31, 635-663.

(43) Rafii-Tabar, H.; Ghavanloo, E.; Fazelzadeh, S. A. Nonlocal Continuum-Based Modeling of Mechanical Characteristics of Nanoscopic Structures. *Phys. Rep.* **2016**, 638, 1-97.

(44) Murmu, T.; Pradhan, S. C. Buckling of Biaxially Compressed Orthotropic Plates at Small Scales. *Mech. Res. Commun.* **2009**, 36, 933-938.

(45) Wang, C. Y.; Murmu, T.; Adhikari, S. Mechanisms of Nonlocal Effect on the Vibration of Nanoplates. *Appl. Phys. Lett.* **2011**, 98, 153101.

(46) Terrones, H.; Lv, R.; Terrones, M.; Dresselhaus, M. S. The Role of Defects and Doping in 2D Graphene Sheets and 1D Nanoribbons. *Rep. Prog. Phys.* **2012**, 75, 062501.

(47) Yang, M. Y.; Huang, J. S. Elastic Buckling of Regular Hexagonal Honeycombs with Plateau Borders under Biaxial Compression. *Comp. Struct.* **2005**, 71, 229-237.

(48) Shenoy, V. B.; Reddy, C. D.; Ramasubramaniam, A.; Zhang, Y. W. Edge-Stress-Induced Warping of Graphene Sheets and Nanoribbons. *Phys. Rev. Lett.* **2008**, 101, 245501.

(49) Jiang, J. W.; Park, H. S. Negative Poisson's Ratio in Single-Layer Graphene Ribbons. *Nano Lett.* **2016**, 16, 2657-2662.

(50) Gu, C.; Gao, G. H.; Yu, Y. X.; Mao, Z. Q. Simulation Study of Hydrogen Storage in Single Walled Carbon Nanotubes. *Int. J. Hydrogen Energy* **2001**, 26, 691-696.

(51) Timoshenko, S. *Theory of Elastic Stability, 2nd ed.*; McGraw-Hill: New York, U.S.A., 1961.

Figures

(a) (b)

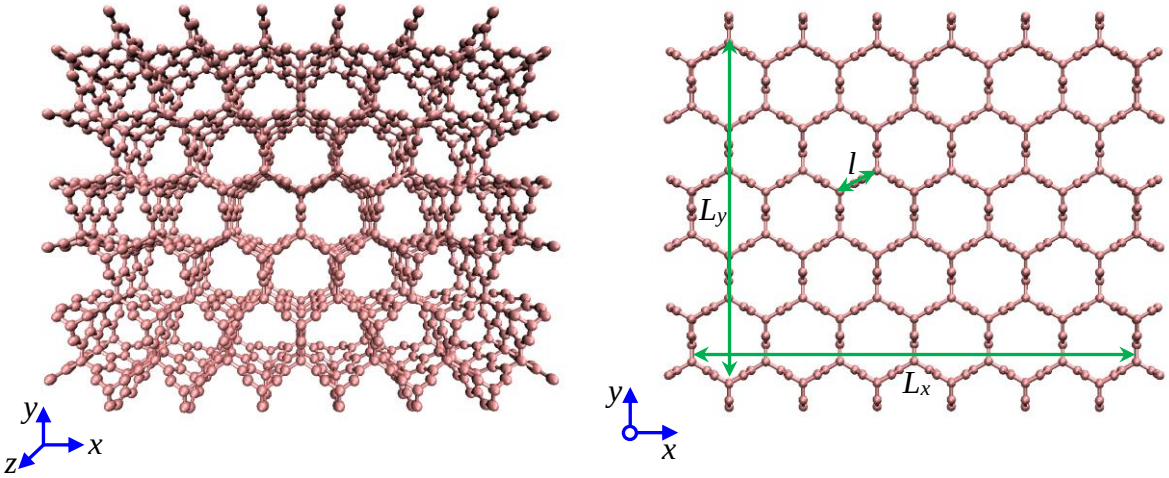

Figure 1. (a) Perspective and (b) front view of the atomic representation of the CHC structure.

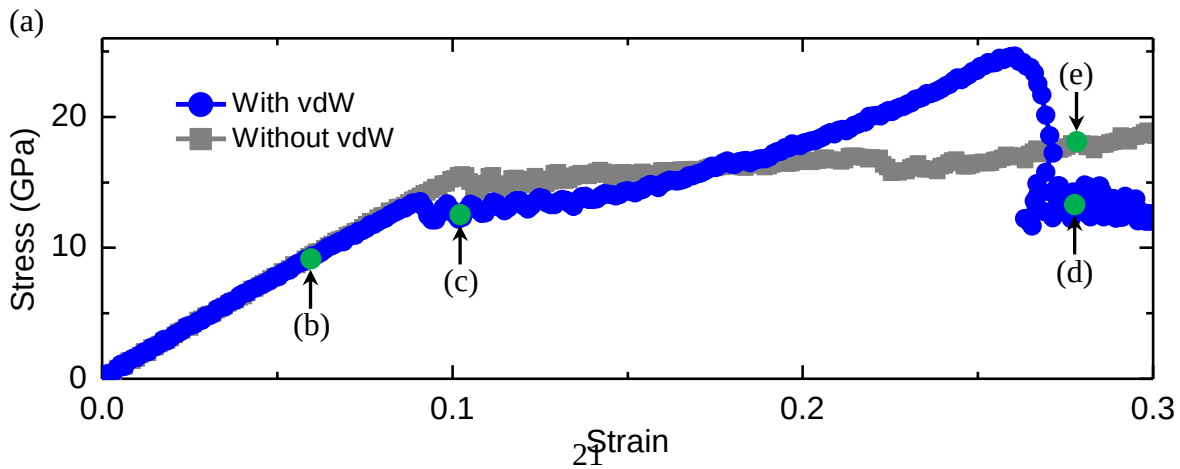

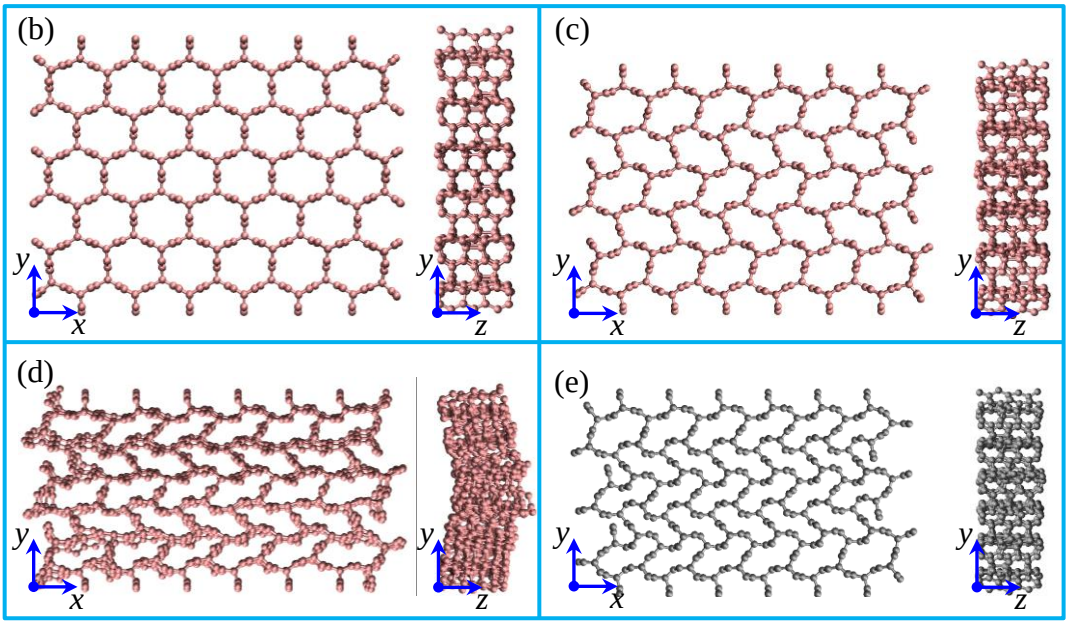

Figure 2. (a) Variation of the stress with respect to the strain for CHCs under the uniaxial compression along the *y* direction. (b)-(e) show the snapshots of representative structures taken at the key points from the stress-strain curve in (a).

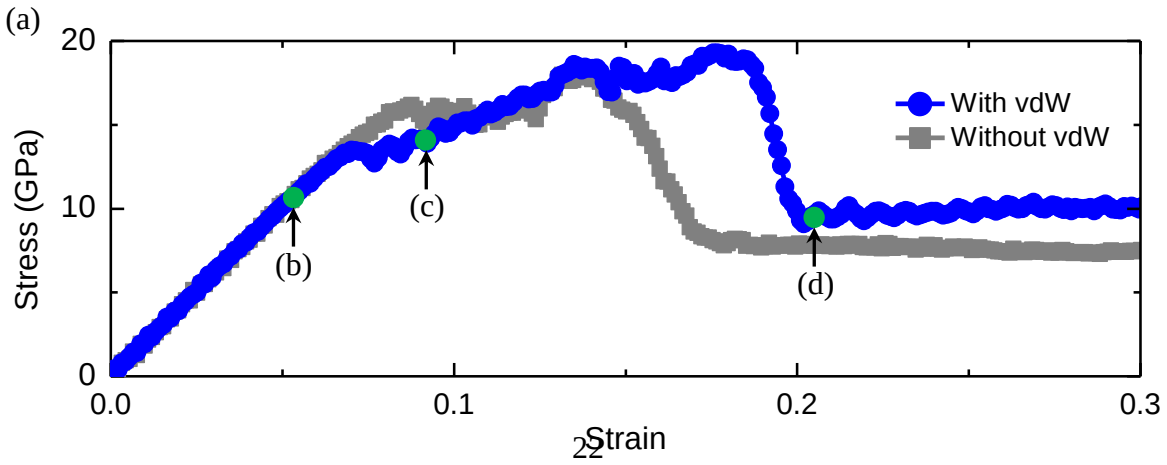

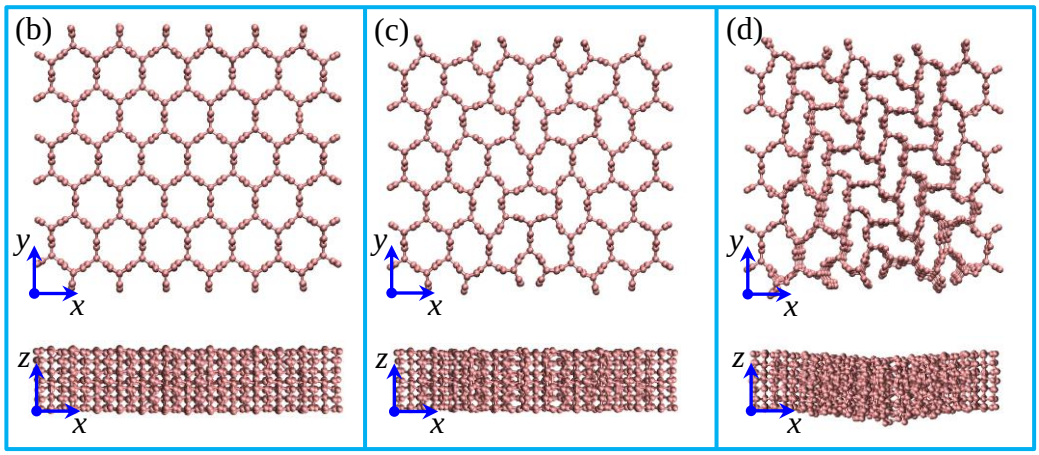

Figure 3. (a) Variation of the stress with respect to the strain for CHCs under the uniaxial compression along the *x* direction. (b)-(d) show the snapshots of representative structures taken at the key points from the stress-strain curve in (a).

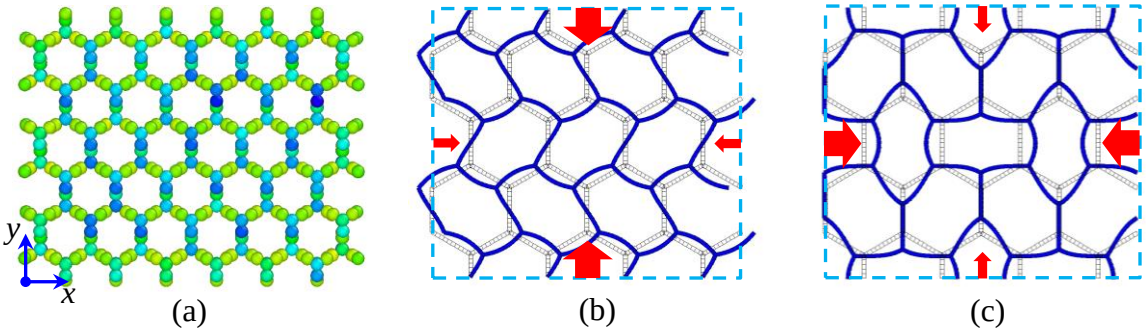

Figure 4. (a) The atomic stress distribution of the CHC after the initial structural relaxation. (b) and (c) are FE simulation results of the buckling modes of a honeycomb structure under the biaxial compression state. Here (b) is the result when $\sigma_{yy} > \sigma_{xx}$, while (c) is the result when $\sigma_{xx} > \sigma_{yy}$.

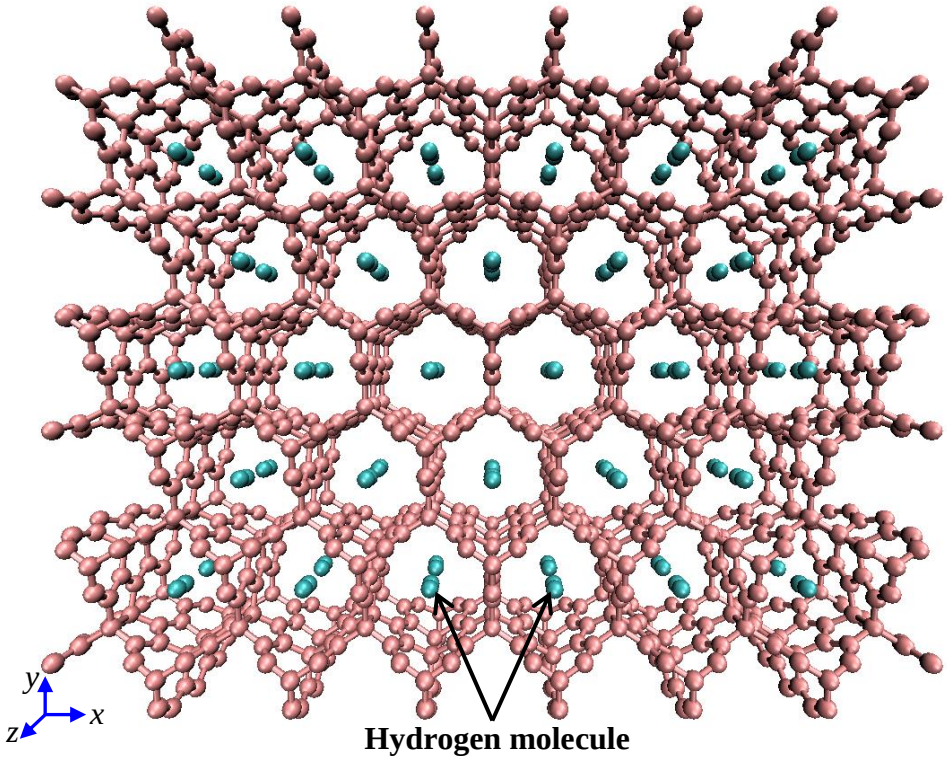

Figure 5. Perspective view of the atomic representation of a CHC structure adsorbed with hydrogen molecules.

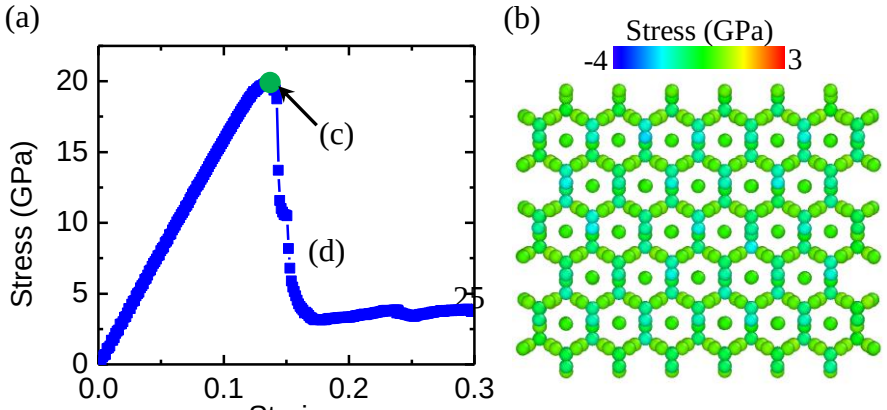

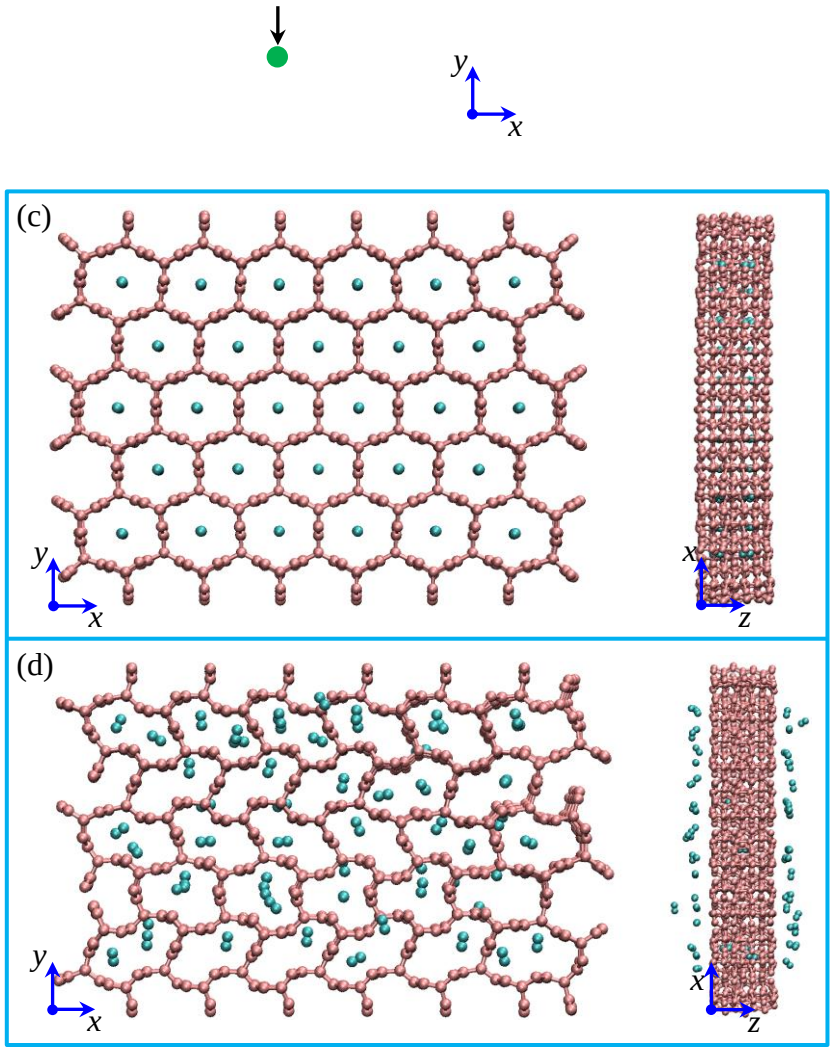

Figure 6. (a) Variation of the stress with respect to the strain for CHCs adsorbed with hydrogen under the uniaxial compression along the *y* direction. (b) The atomic stress distribution of the CHC after the initial structural relaxation. (c) and (d) show the snapshots of the representative structures taken at the key points from the stress-strain curve in (a).

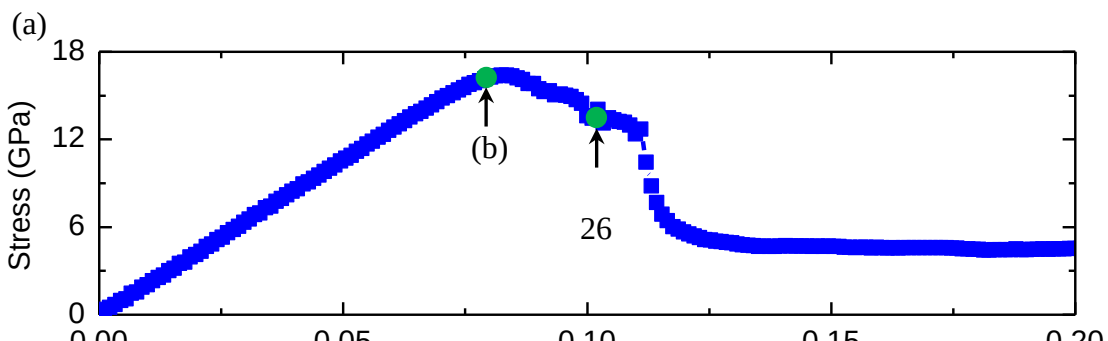

(c)

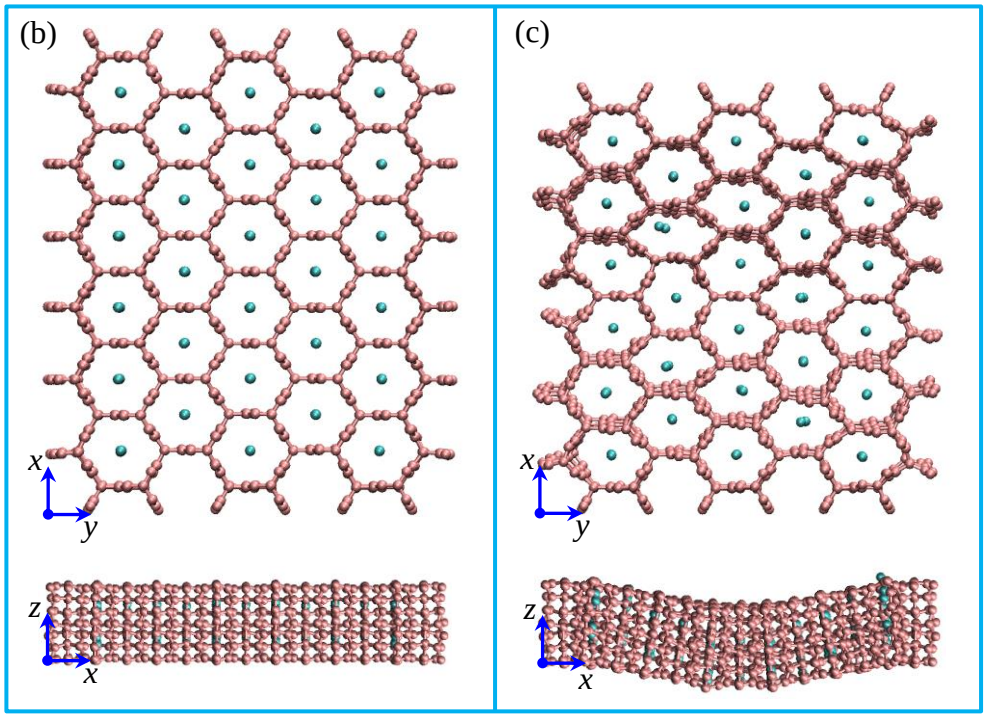

Figure 7. (a) Variation of the stress with respect to the strain for CHCs adsorbed with hydrogen under the uniaxial compression along the *x* direction. (b) and (c) show the snapshots of the representative structures taken at the key points from the stress-strain curve in (a).

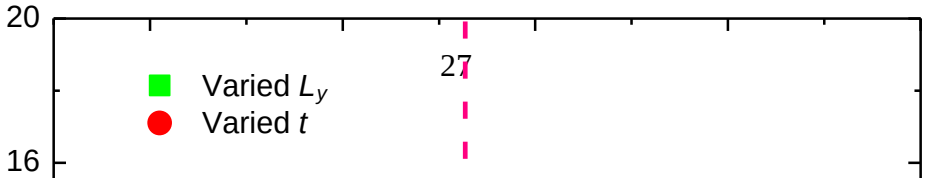

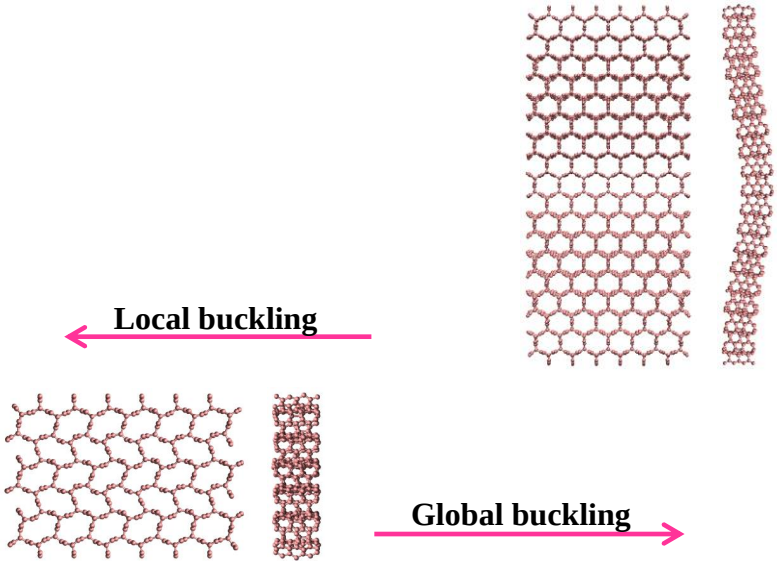

Figure 8. Variation of the critical buckling stress with respect to the length-to-thickness ratio (L_y / t) of CHCs under the uniaxial compression along the y direction. Here the symbols are the MD simulation results and the solid line is the theoretical fitting. The insets show the buckling modes of the local buckling and global buckling of CHCs.

TOC Graphic

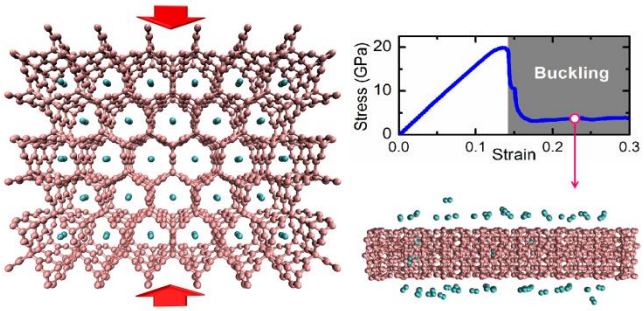
Stress (GPa)
20
10
0
0.0
0.1
0.2
0.3
Strain
Buckling